*VERSION 1.1: December 20, 2006*

# $\phi \rightarrow K^+K^-$ analysis in Run4 Au+Au collisions at 200 GeV energies using BRAHMS spectrometer

Dipali Pal

University of Kansas

# 1 Introduction

In this analysis note, we describe the procedures used to derive the yield dN/dy, temperature T, and spectral shape of the $\phi$ mesons in $K^+K^-$ decay channel in the BRAHMS experiment. We present the yield of the $\phi$ particles from Mid-Rapidity Spectrometer (MRS). The data from Run4 200 GeV Au+Au collisions have been analyzed and presented.

# 2 Data Selection

## 2.1 Event selection

For this analysis, we select events with $|z_{vertex}| < 40$ cm that satisfies MRS trigger conditions. In this way, we obtain about 48 M events at the MRS angle of $40^o$ and magnet current of 1050.

## 2.2 Track selection and particle identification

In order to optimize the statistics and obtain best tracks in our analysis, following single track selection criteria are applied:

1. Tracks reconstructed by TPM1-TPM2-TOFW subsystems,
2. Momentum range: $0.4 <$ p (GeV/c) $< 2$,
3. PID selection: Tracks within $\pm 2\ \sigma$ PID band of the mass-squared distributions around the kaon peak.

In addition to the single track cuts, we eliminate the track pairs that share hits on the same TOF slat as in that case the timing information associated with both tracks are screwed up.

## 2.3 Kaon identification

Kaons are identified by the Time-Of-Flight Wall (TOFW) detector at the MRS. TOFW has an intrinsic timing resolution of $\sim$ 80 ps which facilitates pion/kaon separation upto a momentum of 2 GeV/c for $2\sigma$ PID bands.

The PID selection is performed by analyzing the mass-squared distributions of the tracks:

$$m^2 = p^2(\frac{c^2t^2}{L^2} - 1) \tag{1}$$

where p, t and L represents momentum, time-of-flight and path length of the track.

After reconstructing the $m^2$ distributions of the tracks at different momentum slices, Kaon identification is done in the following steps:

1. Fitting mass-squared distributions with double Gaussian function at different momentum zones within a range of 0.16 - 0.4 GeV$^2$/c$^4$.
2. Parametrizing the gaussian fit centroids ($< m^2 >$) and sigmas ($\sigma$) with second order polynomial function as a function of momenta (p).

3. Defining kaon PID function as:

$$isKaon = \frac{m^2_{measured} - < m^2_{parametrized} >}{\sigma_{parametrized}} \tag{2}$$

In this way, we can identify kaons within $\pm$n$\sigma$ bands. In this analysis, $n = 2$.
Fig 1 shows mass-squared distribution of the positive tracks within 0.1 < $m^2$ ($GeV^2/c^4$) < 0.4 within a momentum range of p = 1.0 - 1.1 GeV/c. This distribution (and distributions for other momentum ranges) is fitted with a double Gaussian function where signal and background both fitted with Gaussian function.

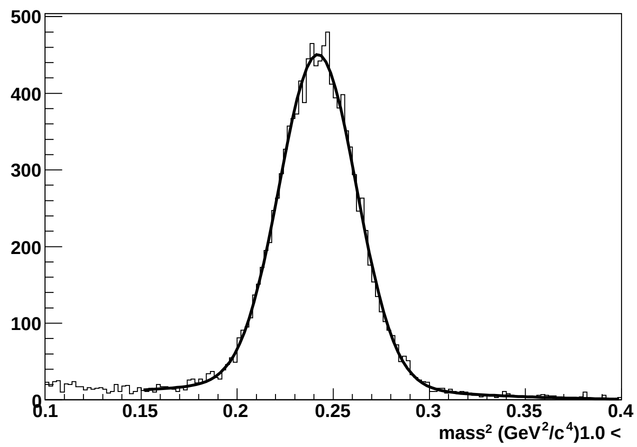


Figure 1: Mass-squared distribution of the positive tracks within 0.1 < $m^2$ < 0.4 $GeV^2/c^4$ and 1.0 < p <1.1 GeV/c.

This exercise is then repeated for different momentum bins. The centroids and $\sigma$'s of the $m^2$ distributions are then plotted as a function of momentum and fitted with second order polynomial function in p to determine $< m^2_{parametrized} >$ and $\sigma^2_{parametrized}$ in eqn. (2).
Figs 2 and 3 show centroids and sigmas of the fitted mass-squared distributions as function of momenta for the positive and negative tracks of the polarity "A" data.
Similarly, Figs 4 and 5 show centroids and sigmas of the fitted mass-squared distributions as function of momenta from the positive and negative tracks of the polarity "B" data.
Finally, Figs. 6 - 11 demonstrate the kaon PID where we superimposed the mass-squared distributions of identified $K^+$'s within 2 sigma PID band on all tracks for four momentum ranges from the "A" polarity data. The figures 6 - 11 indicate clear kaon identification within the range of 0.4 < p (GeV/c) < 2.0. Same quality of kaon identification has been observed for negative tracks from the polarity "A" and positive and negative tracks from polarity "B" datasets.

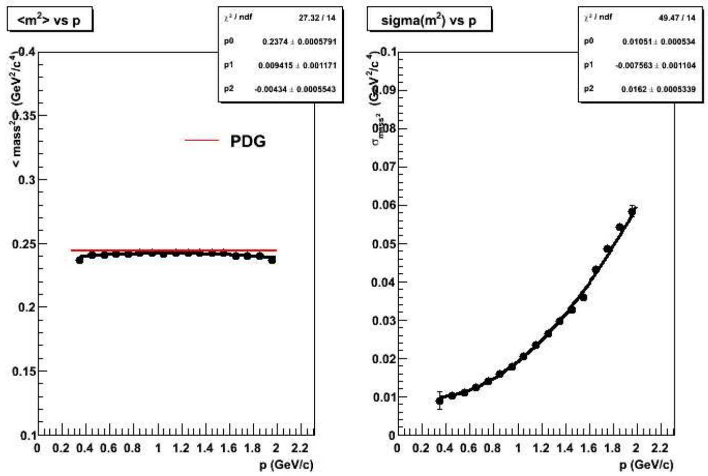


Figure 2: Variation of centroids (left) and sigmas (right) with track momenta for positive tracks from polarity "A" data.

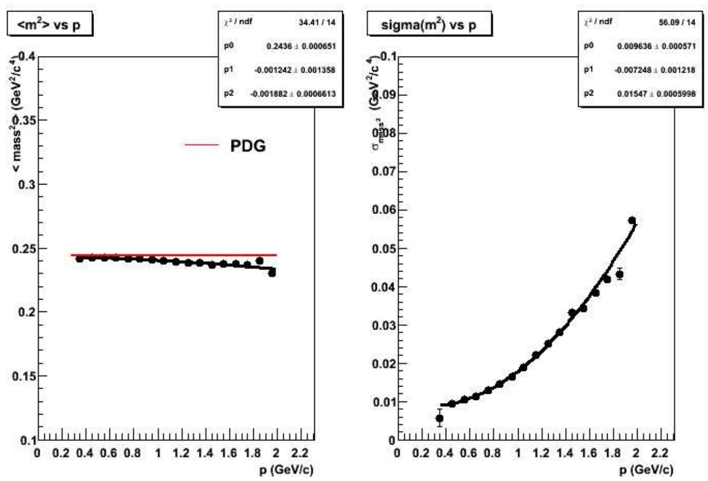


Figure 3: Variation of centroids (left) and sigmas (right) with track momenta for negative tracks from polarity "A" data.

# 3 $K^+K^-$ invariant mass distribution

In this section, we describe the procedure of the $\phi$ meson reconstruction in $K^+K^-$ decay channel. We combine all $K^+$ and $K^-$ from the same events which constructs the measured invariant mass distribution (S). This has a large combinatorial background. The combinatorial background is estimated by event mixing technique. Here $K^+$ from an event is combined with $K^-$ from the next 10 events within the same centrality, vertex and trigger class. The mixed event invariant mass spectrum (M) is then normalized to the same event distribution above the $\phi$ mass region. This

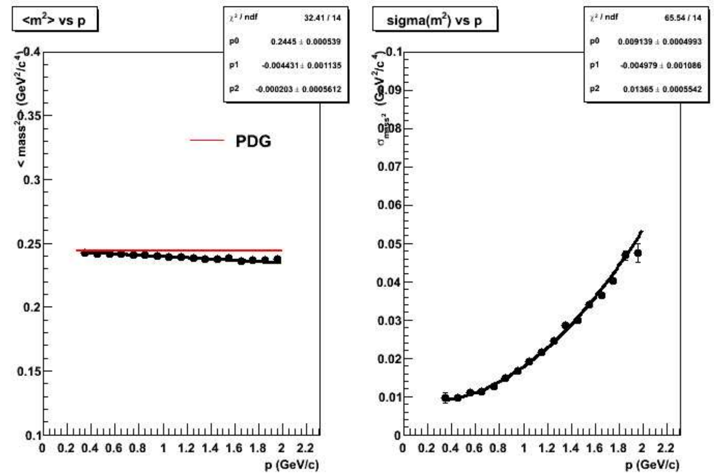


Figure 4: Variation of centroids (left) and sigmas (right) with track momenta for positive tracks from polarity "B" data.

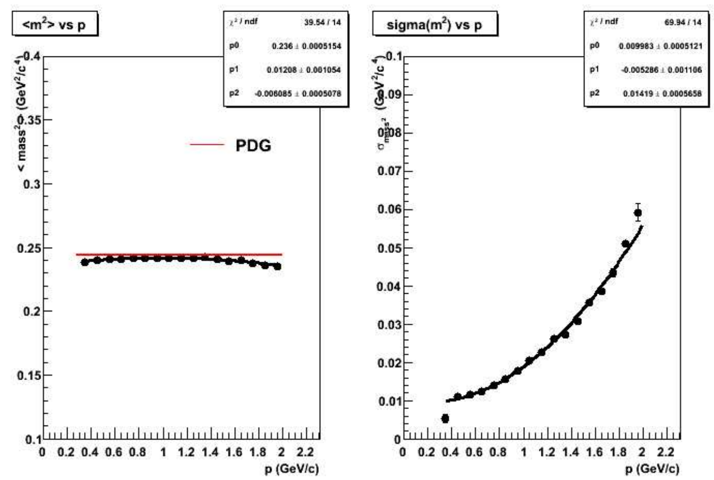


Figure 5: Variation of centroids (left) and sigmas (right) with track momenta for negative tracks from polarity "B" data.

gives the combinatorial background (B). Finally, we subtracted the combinatorial background from the measured invariant mass distribution to extract the $\phi$ signal:

$$Signal = S - B \tag{3}$$

The $\phi \rightarrow K^+K^-$ mass spectra is shown in Fig. 12 where we reconstruct about 123 $\phi$ mesons in MRS. The spectrum is fitted with relativistic Breit-Wigner function to extract the centroid and width both of which are found to be consistent with the particle data book within errors.

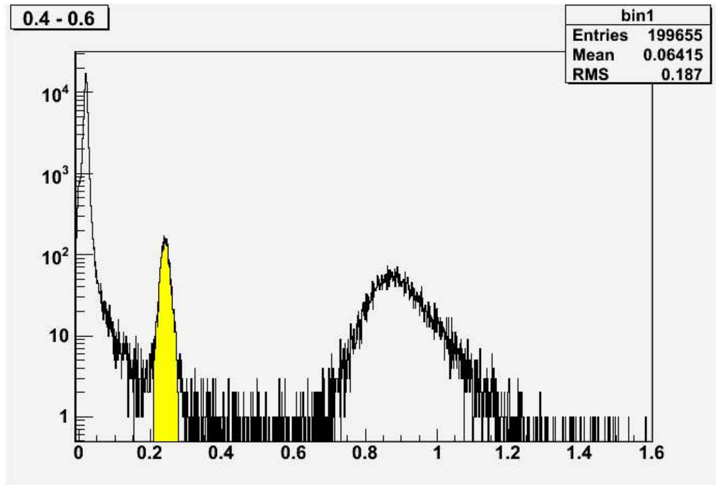


Figure 6: Mass-squared distribution of all positive tracks and identified $K^+$ tracks within 2 sigma PID bands within 0.4 < p (GeV/c) < 0.6.

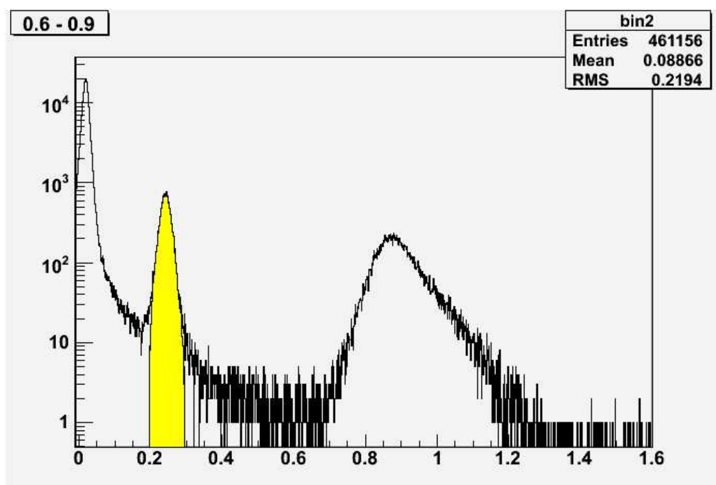


Figure 7: Mass-squared distribution of all positive tracks and identified $K^+$ tracks within 2 sigma PID bands within 0.6 < p (GeV/c) < 0.9.

# 4 $\phi$ meson yield analysis

In this section we shall describe the extraction of dN/dy and temperature (T) of $\phi$ mesons in Run4 Au+Au collisions.

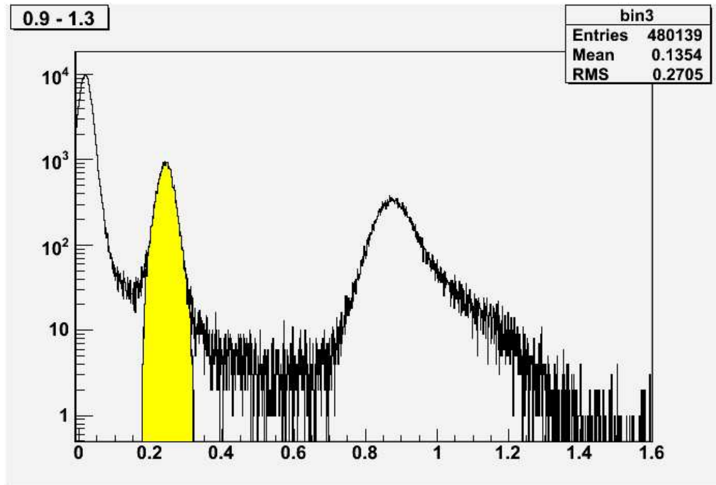


Figure 8: Mass-squared distribution of all positive tracks and identified $K^+$ tracks within 2 sigma PID bands within $0.9 <$ p (GeV/c) $< 1.3$.

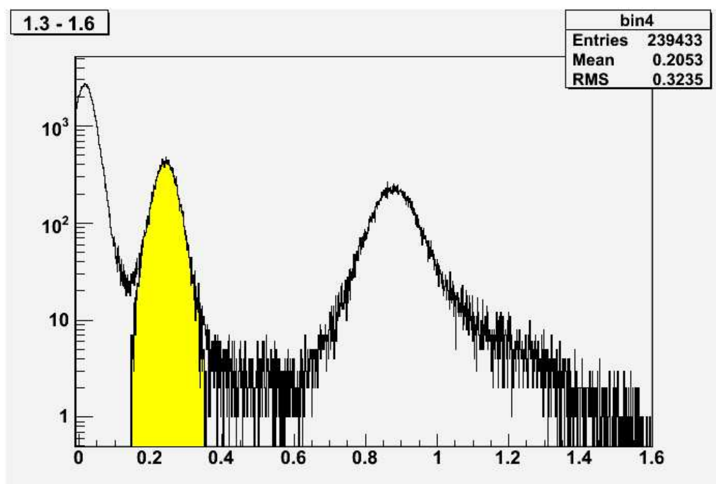


Figure 9: Mass-squared distribution of all positive tracks and identified $K^+$ tracks within 2 sigma PID bands within $1.3 <$ p (GeV/c) $< 1.6$.

## 4.1 Method

The basic strategy in this analysis is to construct transverse mass distribution of the reconstructed $\phi$ mesons and to fit that with exponential function to extract dN/dy and the inverse slope, T as two fitting parameters.

In order to obtain the $\phi$ meson transverse mass ($m_T$) spectrum, we extracted the $\phi$ meson raw yields within four $m_T$ bins,
(a) $1.2 < m_T(GeV/c^2) < 1.8$,

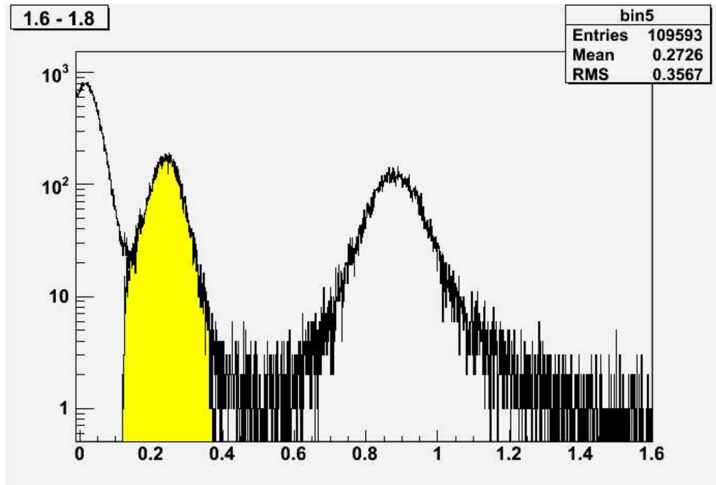


Figure 10: Mass-squared distribution of all positive tracks and identified $K^+$ tracks within 2 sigma PID bands within 1.6 < p (GeV/c) < 1.8.

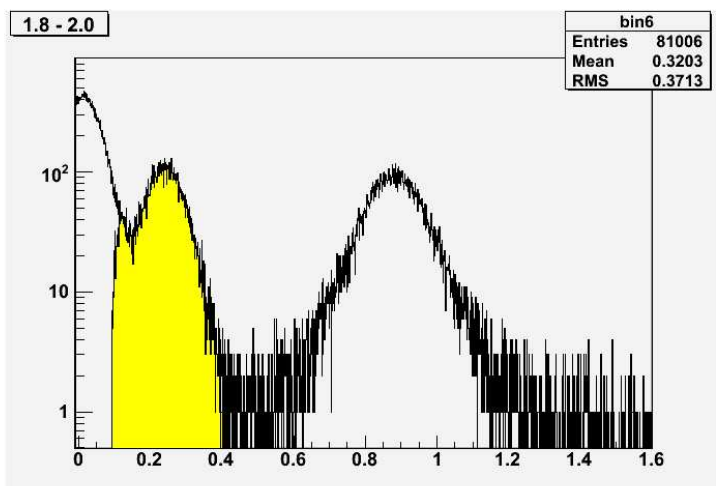


Figure 11: Mass-squared distribution of all positive tracks and identified $K^+$ tracks within 2 sigma PID bands within 1.8 < p (GeV/c) < 2.0.

(b) $1.8 < m_T(GeV/c^2) < 2.0$,
(c) $2.0 < m_T(GeV/c^2) < 2.2$, and
(d) $2.2 < m_T(GeV/c^2) < 2.5$.

For making the $m_T$ spectra, we subtracted the combinatorial background (CB) from the same event transverse mass distributions in different $m_T$ bins within the $\phi$ mass window of 1.013 - 1.031 GeV/$c^2$. This constituted the raw $m_T$ distribution:

$$N_{\phi}^{raw}(m_T) = N_{same\ event}^{K^+K^-} - N_{CB}^{K^+K^-} \tag{4}$$

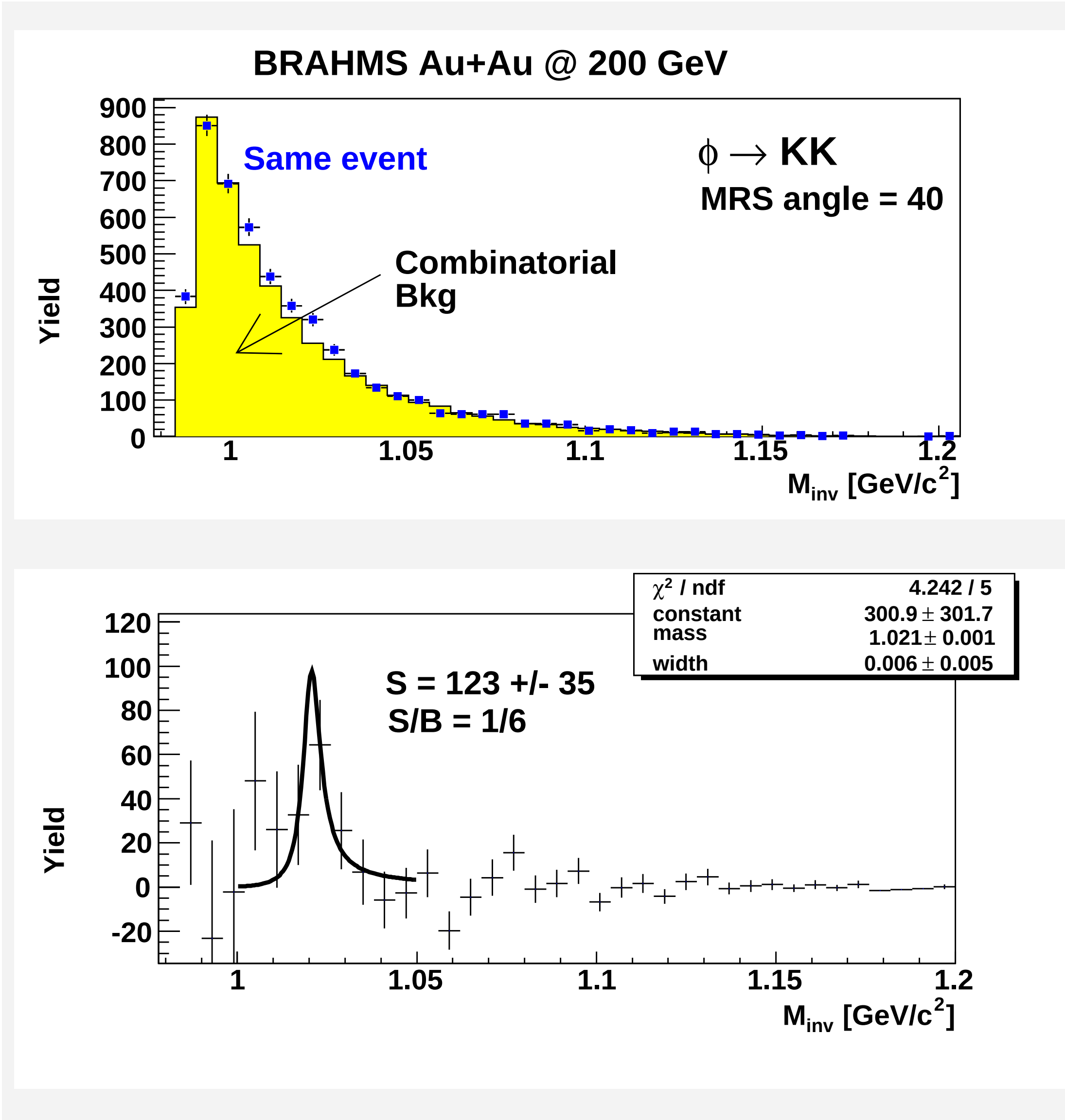


Figure 12: Invariant mass distributions. Up: Measured and combinatorial mass distributions. Down: Subtracted mass spectrum showing a clear $\phi$ meson peak fitted with relativistic Breit-Wigner distribution.

This bin-by-bin yield is then corrected for efficiencies due to detector acceptance and dead area ($CF$), pair occupancy ($\epsilon_{pair-embedding}$), and run-by-run yield variations ($\epsilon_{run-by-run}$), The corrected yield in each $m_T$ bin is

$$N_{\phi}(m_T) = \frac{N_{\phi}^{raw}(m_T) \times CF(m_T)}{N_{event} \times \epsilon_{pair-embedding} \times \epsilon_{run-by-run}} \tag{5}$$

We use MRS trigger conditions for both data and monte-carlo so that the minimum bias conversion factor in both cases remain the same.

Now, in order to derive the invariant yield, $(1/2\pi m_T) \times d^2N/dm_T dy$, $N_\phi(m_T)$ is divided by $2\pi$, $m_T$ bin centroid and $m_T$ bin-size.

The statistical error bar on each data point shown here is calculated by the standard propagation of error technique as described below.

The $\phi$ signal is given by:

$$S = R - B, \tag{6}$$

where R is the yield in the same event invariant mass spectrum and B is the combinatorial background under $\phi$ peak ($1.013 \leq M_{inv} \leq 1.031\ GeV/c^2$). Now, the error in S is

$$\Delta S = \sqrt{(\Delta R^2 + \Delta B^2)}, \tag{7}$$

where

$$\Delta R = \sqrt{R}, \tag{8}$$

and

$$\Delta(B)/B = \sqrt{([\Delta(C)/C]^2 + [\Delta(D)/D]^2)}; \Delta(B) = B \times \sqrt{([\Delta(C)/C]^2 + [\Delta(D)/D]^2)} \tag{9}$$

$\Delta B$ is computed by standard propagation of error technique.

## 4.2 Acceptance correction: Monte Carlo

In order to determine $\phi$ - meson invariant yields at different $m_T$ bins, the raw $\phi$ yield are then corrected for acceptance of the MRS. This is done by Monte-Carlo simulation. We have processed 150 M single $\phi \rightarrow K^+K^-$ pair Monte Carlo for MRS.

We generated events using the single particle event generator (EXODUS) with the following specifications:

a) flat rapidity distribution within 0 < y < 2 and uniform azimuthal angle, $\phi$: 0 - $2\pi$.

b) flat z-vertex distribution within $|z| < 40$ cm.

c) $p_T$ distribution of the $\phi$ mesons according to:

$dN/dp_T = p_T$ exp(-$m_T/(t_{f_o} + \beta^2 m_\phi)$)

with $t_{f_o} = 0.157$ GeV and $\beta = 0.4$, i.e, an effective slope of T = 0.320 GeV.

We decay the $\phi$ mesons within the generator and stored the resulting outputs into ascii OSCAR file.

The invariant mass and transverse mass distribution of the input $\phi$ mesons reconstructed through $K^+K^-$ channel is shown in Figs. 13 and 14 respectively.

The decay kaon pairs are then passed through the generated events through the BRAHMS simulation package, BRAG, based on GEANT and then propagating the BRAG outputs through the data reconstruction chain; Finally, we computed the acceptance correction factors defined as the generated/reconstructed ratios at the above $m_T$ bins.

For derivation of correction factors, we use the identical analysis code with data.

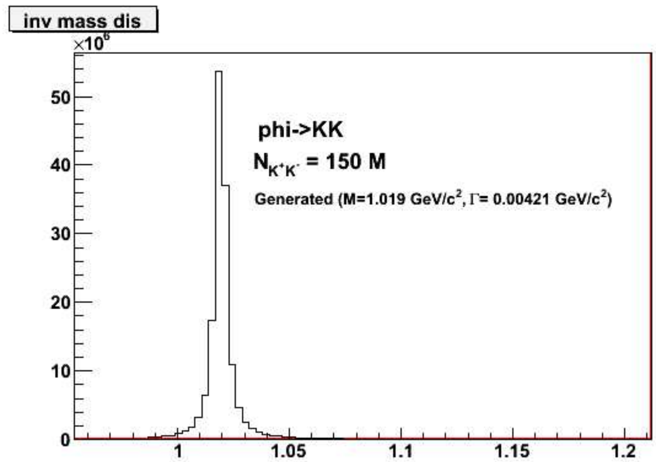


Figure 13: Invariant mass spectra of $K^+K^-$ pairs from $\phi$ generated by EXODUS event generator

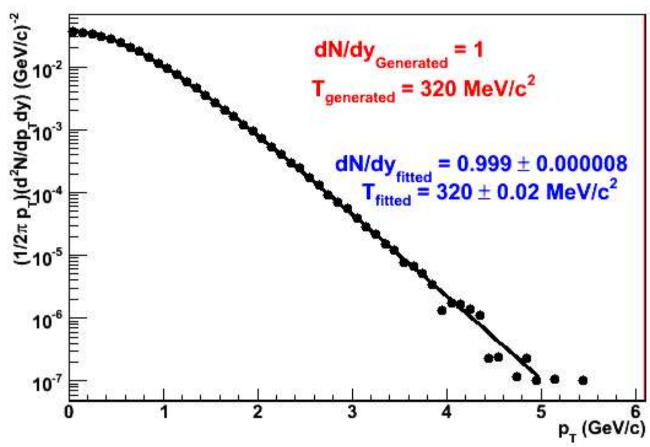


Figure 14: Transverse momentum spectra of $\phi \rightarrow K^+K^-$ pairs mesons generated by EXODUS event generator

Figs. 16 - 15 represent PID parameters for monte-carlo each of which plots centroids and sigmas of the mass-squared distributions as function of momenta.

The acceptance correction factor (CF) is given by:

$$CF = \frac{N_{\phi}^{Generated}(0 < y < 2)}{2 \ \times \ N_{\phi}^{Reconstructed}} \tag{10}$$

Here, the factor of 2 in the denominator ensures that the correction factor is calculated per unit of rapidity. The correction factors calculated in this way include acceptance and reconstruction efficiencies.

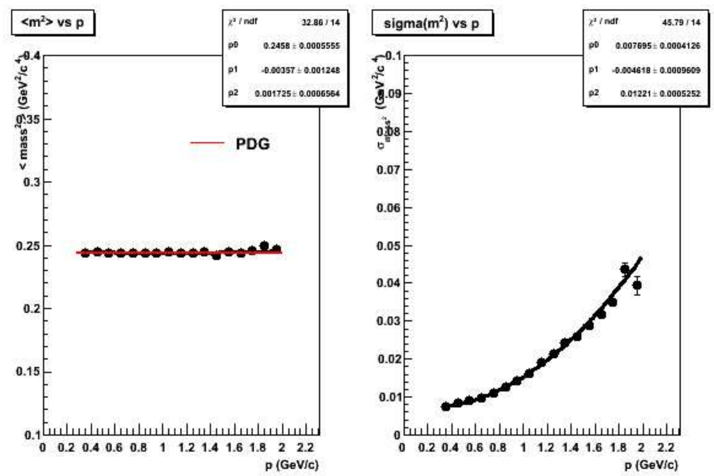


Figure 15: PID parametrization in Monte-Carlo for positive tracks. Centroids vs p (left) and sigmas vs p (right).

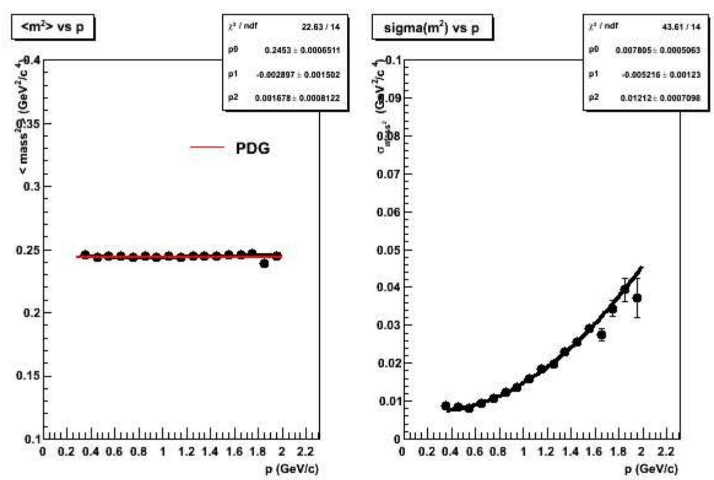


Figure 16: PID parametrization in Monte-Carlo for negative tracks. Centroids vs p (left) and sigmas vs p (right).

Fig 17 shows the acceptance correction factors as function of transverse mass of the $\phi$ mesons. We have multiplied the correction factor with the raw $m_T$ distribution of $\phi$ meson reconstructed from the data to derive the "acceptance corrected" spectra.

## 4.3 Run by run efficiency ($\epsilon_{run-by-run}$)

The run-by-run variation of the dead channels and efficiencies is considered by calculating a run-by-run correction factor as follows.

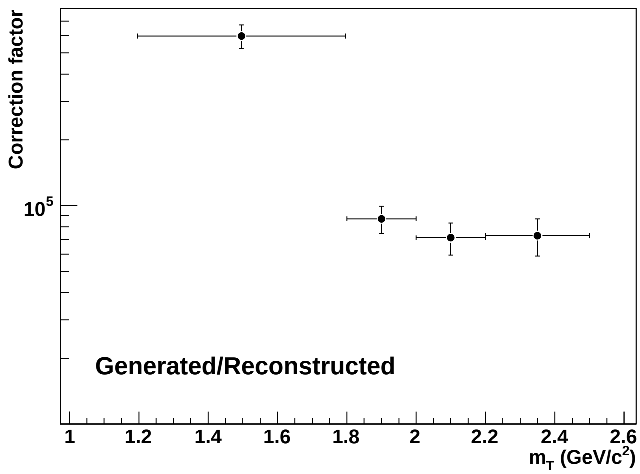


Figure 17: Acceptance correction factors vs momentum of the $K^+K^-$ pairs from the $\phi$ mesons.

We calculate the number of tracks per event in each run as:

$$A_{track} = \frac{N_{track}}{N_{event}} \tag{11}$$

Using the above numbers, we compute run by run single track efficiency with reference to the average number of tracks per events calculated over the full range of runs used in this analysis as:

$$\epsilon_{track} = \frac{A^{average}_{track}}{A_{track}} \tag{12}$$

Finally, we calculate an average of $\epsilon_{track}$ weighted over the number of events in each run as:

$$< \epsilon_{track} >= \frac{\Sigma \epsilon^{run}_{track} \times N^{run}_{event}}{\Sigma N^{i}_{event}} \tag{13}$$

The summation is carried out over all runs.

This is the average run-by-run efficiency for the single tracks. To account for the pairs, we calculated the efficiencies of the positive and negative tracks through TPC1-TPC2-TOFW in MRS using eqn. (13) and multiplied them with each other:

$$< \epsilon_{pair} >= \epsilon^{+} \ \times \ \epsilon^{-} \tag{14}$$

Fig 18 shows the number of positive (left) and negative (right) tracks per event as a function of the run number.

The run by run efficiency for the positive and negative tracks derived in the above method are 0.9952 and 0.9998 respectively making a pair efficiency of 0.9952 $\times$ 0.9981 = 0.9950.

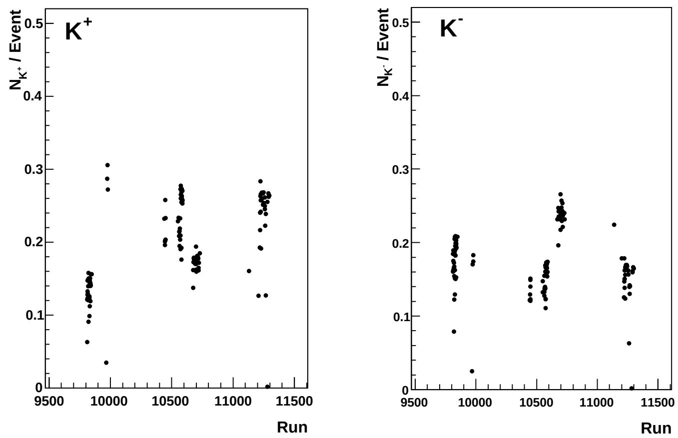


Figure 18: Number of positive (left) and negative (right) tracks per event vs run number.

## 4.4 Occupancy dependent correction

The occupancy (multiplicity) dependent corrections are done by embedding the monte-carlo tracks into the real data. We have used the same occupancy dependent corrections for the kaon tracks as Run2 analysis where the efficiency was found to be a function of the number of TPC1 hits [1]:

$$\epsilon_{occupancy}^{single} = 0.952 - 7.2 \times 10^{-5} . H \tag{15}$$

where $H$ is the number of TPC1 hits. For minimum bias events the average number of TPC1 hits is 88. This gives us a single kaon occupancy dependent efficiency correction factor of 0.95 with a statistical uncertainty of about 0.002. Since we are considering kaon pairs, the pair occupancy efficiency is $\epsilon_{occupancy}^{pair} = {\epsilon_{occupancy}^{single}}^2 = 0.90 \pm 0.004$.

## 4.5 Results

The minimum-bias transverse mass spectra is shown in Figure 19.

However, we fitted the $m_T$ spectrum with exponential function

$$\frac{1}{2\pi m_T}\frac{d^2N}{dm_T dy} = \frac{dN/dy}{2\pi T(T + M_\phi)} e^{-(m_T - m_\phi)/T} \tag{16}$$

The centroid of each $m_T$ bin is calculated iteratively by

$$< m_T >= \frac{\int m_T.exp(-m_T/T)}{\int exp(-m_T/T)} \tag{17}$$

where T is the inverse slope extracted from the fitting of the $m_T$ spectrum.

dN/dy and T are extracted as two parameters from the fitting which is shown in Table 1

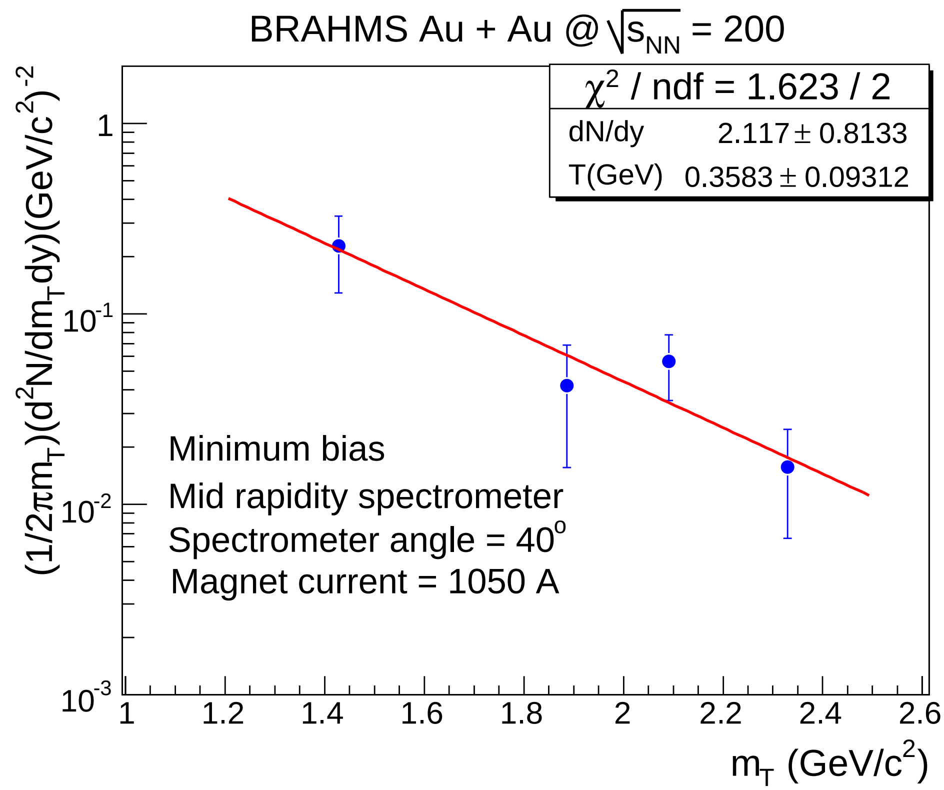


Figure 19: Minimum-bias transverse mass distribution.

Table 1: Yield parameters dN/dy and T.

| dN/dy | T (MeV) |
|---|---|
| $2.12 \pm 0.81$ | $358 \pm 93$ |

In order to compare the BRAHMS $\phi$ meson result with Run2 STAR data, we do the following exercise. First, consider the BRAHMS single kaon data [2] where we find $(\mathrm{dN/dy})_{y\,\sim\,1} \approx 41$ and $(\mathrm{dN/dy})_{y\,\sim\,0} \approx 45$. That means if we move from y=0 to y=1, there is about 10% drop in the yield. Now, consider STAR $\phi$ meson data [3], where we can find the minimum-bias (0-80%) dN/dy of the $\phi$ mesons at y=0 as $2.40 \pm 0.07$. If we now go to y=1, then we expect to observe a 10% drop in the $\phi$ yield which means the projected $\phi$ meson yield at y=1 should be $2.16 \pm 0.06$. In BRAHMS, we observe the $\phi$ yield at y $\approx$ 1 to be $2.12 \pm 0.81$ which is consistent with the projected $\phi$ yield just described.

## 4.6 Systematic Errors

The study of systematic errors on dN/dy and T is based on the following points:
a) Normalization of the combinatorial background ($\delta^{sys}_{norm}$),
b) Effect of mass window for $\phi$ meson reconstruction in both data and MC ($\delta^{sys}_{mass}$),
c) Fitting range ($\delta^{sys}_{range}$) and fitting function ($\delta^{sys}_{func}$) of the $m_T$ spectra,

To derive the systematic error for each case, we first determine the maximum deviation with respect to the measured values of dN/dy and T and then divide it by $\sqrt{12}$. The factor $\sqrt{12}$ came as a combination of a factor of 2 because of the min-to-max extent assuming symmetry, and $\sqrt{3}$ from a box around a Gaussian.

Finally, we calculated the total systematic error as,

$$\delta^{sys} = \sqrt{(\delta^{sys}_{norm})^2 + (\delta^{sys}_{mass})^2 + (\delta^{sys}_{range})^2 + (\delta^{sys}_{func})^2} \quad (18)$$

### 4.6.1 Systematics of normalization of the combinatorial background ($\delta^{sys}_{norm}$)

The $\phi$ meson peak is extracted by subtracting the combinatorial background from the same event (measured) invariant mass distribution. The combinatorial background is determined by event mixing method described earlier in this note. The mixed event distribution is normalized to the measured mass distribution above the $\phi$ meson mass range where we do not expect to see any real correlation. This normalization, however, has systematic uncertainties. To study the systematics of normalization, we normalized the mixed event spectrum within different mass regions, namely
(a)$1.11 \leq M_{inv}(GeV/c^2) \leq 1.5$,
(b)$1.10 \leq M_{inv}(GeV/c^2) \leq 1.5$,
(c)$1.09 \leq M_{inv}(GeV/c^2) \leq 1.5$,
(d)$1.08 \leq M_{inv}(GeV/c^2) \leq 1.5$,
We calculated then number of $\phi$ signal under these different mass regions. We then derived the systematic error by considering the maximum deviation with respect to the measured $\phi$ signal.

### 4.6.2 Systematics of $\phi$ mass window ($\delta^{sys}_{mass}$)

The number of $\phi$ is calculated by integrating the yield within a fixed mass window of $\pm$ 9 MeV with respect to the centroid 1.022 GeV/$c^2$ ($1.013 < M < 1.031$ GeV/$c^2$) on the subtracted invariant mass spectra. In case of $m_T$ distributions, we simply subtracted the yields from the same event and mixed event $m_T$ distributions within the above mass window in every $m_T$ bin. We studied the systematics associated with this mass window by varying it in three more sets namely, $\pm$ 6 MeV, $\pm$ 12 MeV, and $\pm$ 15 MeV with respect to $\phi$ mass centroid.

Table 2: Total Systematic error in dN/dy.

| $\delta^{sys}_{norm}$ (%) | $\delta^{sys}_{mass}$ (%) | $\delta^{sys}_{range}$ (%) | $\delta^{sys}_{func}$ (%) | $\delta^{sys}$ (%) |
|---|---|---|---|---|
| 8.7 | 4.9 | 6.8 | 1.54 | 12.18 |

#### 4.6.3 Systematics in the fitting of the $m_T$ spectra

dN/dy for each dataset is extracted by fitting the $m_T$ spectra with exponential function and then extrapolating the fit to $m_T = m_\phi$. Experimentally we can measure a limited $m_T$ range; it is, therefore, important to calculate the systematics associated with the extrapolation. This is done in two ways. First, by fitting the $m_T$ spectra in different fitting ranges and second, by fitting the spectra with different fitting function.

(A)**Systematics due to fitting range ($\delta^{sys}_{range}$)**:

In order to calculate the systematics due to fitting range, we used three fitting ranges:
a) $1.2 < m_T(GeV/c^2) < 2.5$,
b) $1.2 < m_T(GeV/c^2) < 2.2$, and,
c) $1.8 < m_T(GeV/c^2) < 2.5$,

This means we have varied the highest $m_T$ bin keeping the lowest $m_T$ bin fixed and then did the reverse i.e vary the lowest $m_T$ bin keeping the highest one fixed.

(B)**Systematics due to fitting function ($\delta^{sys}_{func}$)**;

In order to study the systematics associated with fitting function, we did a Boltzmann function fit to the $m_T$ spectra. The Boltzmann function can be expressed as:

$$\frac{1}{2\;\pi\;m_T}\;\frac{d^2N}{dm_T dy}\;=\;\frac{(dN/dy).m_T}{2\;\pi\;(T^2+2m_\phi T+2m_\phi^2)}.e^{-(m_T-m_\phi)/T} \tag{19}$$

## 4.7 Total Systematic Error

Considering all these systematic errors, we estimated the net systematic error in dN/dy and T in Tables 2 and 3 respectively.

Table 3: Total Systematic error in T.

| $\delta^{sys}_{mass}$ (%) | $\delta^{sys}_{range}$ (%) | $\delta^{sys}_{func}$ (%) | $\delta^{sys}$ (%) |
|---|---|---|---|
| 7.0 | 5.32 | 4.60 | 9.92 |

# 5 Summary

We have reconstructed the $\phi$ mesons in $K^+K^-$ decay channel using the MRS subsystem of the BRAHMS spectrometer. The invariant mass spectrum and transverse mass spectrum have been extracted from the data. The yield parameters dN/dy and T are given by $2.12 \pm 0.81(stat) \pm 0.26(sys)$ and $358 \pm 93(stat) \pm 36(sys)$ MeV respectively.

# References

[1] Masters thesis, Truls Martin Larsen, 2003, http://www4.rcf.bnl.gov/brahms/WWW/thesis/brahms_tpc_eff.pdf.

[2] BRAHMS Collaboration, Phys. Rev C72, 014908 (2005).

[3] STAR Collaboration, Phys. Lett. B 612 (2005) 181.